

**Current Practice and Recent Developments in
Wall Functions II
(Advanced Approaches)**

**Dr Hector Iacovides
Department of Mechanical Aerospace and
Manufacturing Engineering
UMIST**

CONTENTS

1. Limitations of Conventional Wall Functions.
2. Refinements of the Conventional Wall Function.
3. Advanced wall functions.
 - 3.1 The Analytical Wall Function.
 - 3.2 The Numerical Wall Function.
4. Concluding Remarks.

1. Limitations of Conventional Wall Functions.

The conventional wall functions introduced in the earlier lecture rely on the following assumptions:

1. Near-wall velocity obeys the log-law.
2. The total shear stress remain constant over the near-wall control volume.
3. Within the fully turbulent region of the near-wall control volume, the turbulent kinetic energy remains constant.
4. The dissipation rate is inversely proportional the wall distance over the inner region and constant across the viscous sub-layer.
5. In three-dimensional flows the velocity direction remains unchanged between the near-wall node and the wall.

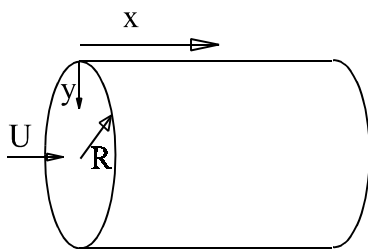
To appreciate how limiting these approximations are, it would be instructive to:

Examine the effect of the departure from the uniform stress

Identify under what circumstances some of the other assumptions no longer apply.

Departures from uniform-stress behaviour.

In fully developed internal flows, such as pipe or channel flows, the total shear stress (viscous + turbulent) varies linearly from τ_w at the wall to zero at the symmetry axis, or plane. This may be readily shown for pipe flow as follows.



U- Momentum Equation for fully developed conditions :

$$\frac{1}{r} \frac{\partial}{\partial r} \left(\mu \frac{\partial U}{\partial r} - \rho \overline{uv} \right) \equiv \frac{1}{r} \frac{\partial}{\partial r} (\tau) = - \frac{\partial P}{\partial x} = \text{Constant}$$

Integration, w.r.t. r, with $\tau = \tau_w$ at $r = R$ and $\tau = 0$ at $r = 0$, then leads to :

$$\tau = \tau_w r / R = \tau_w (R-y)/R$$

At **high mean flow Reynolds numbers** ($Re \equiv U_B \cdot D / \nu$) the viscous sub-layer is thin enough for the reduction in shear stress across it to be negligible.

The approximation of uniform stress in the inner region is thus reasonable.

Consequently in fully-developed pipe and channel flows, the at high Re values, the near-wall flow obeys the log-law.

At **low Reynolds numbers**, because for a given value of y^+ ($\equiv yU_\tau / \nu$), the physical distance, y , becomes greater, the thickness of the viscous sub-layer increases.

The percentage reduction in shear stress across the sub-layer therefore increases.

This causes a departure from the uniform shear stress condition/

This in turn leads to deviations from the log-law. In terms of wall co-ordinates (y^+) the viscous sub-layer becomes thicker.

This reduction in shear stress is more conveniently expressed in terms of $d\tau^+/dy^+$. Where $\tau^+ \equiv \tau/\tau_w$.

$$\text{Since : } \tau = \tau_w (R-y)/R \quad \rightarrow \quad d\tau^+ / dy = - 1 / R$$

$$\rightarrow \quad d\tau^+ / dy^+ = - v / U_\tau R = - 2 (v/U_B \cdot D) (\rho U_B^2 / \tau_w)^{0.5}$$

$$d\tau^+ / dy^+ = - 2 \text{Re}^{-1} (\tau_w / \rho U_B^2)^{-0.5}$$

Introduction of Blasius correlation

$$\tau_w / \rho U_B^2 \approx 0.04 \text{Re}^{-1/4} \quad \text{results in :}$$

$$d\tau^+ / dy^+ = - 10 \text{Re}^{-7/8}$$

Since for $\text{Re} > 10,000$ the mean velocity follows the log-law, it can be concluded that **departures from the uniform stress limit** are caused when :

$$d\tau^+ / dy^+ < - 3 \times 10^{-3}$$

An increase in the negative shear stress gradient, can be caused by a number of reasons.

NEGATIVE PRESSURE GRADIENT

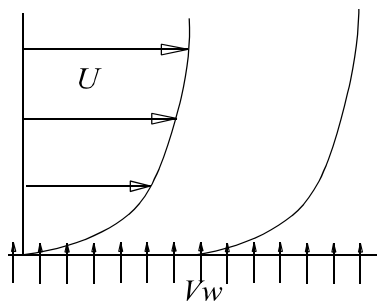
For such a boundary layer (accelerating), the momentum equation is reduced to :

$$\frac{\partial \tau}{\partial y} - \frac{\partial P_{\infty}}{\partial x} = 0 \quad \rightarrow \quad \frac{d\tau^+}{dy^+} = \frac{v}{\rho U_{\tau}^3} \frac{\partial P_{\infty}}{\partial x}$$

STRONGLY HEATED INTERNAL FLOWS

Strong heating causes a reduction in fluid density. As a result, the flow accelerates again causing a reduction in total shear stress across the sub-layer.

BOUNDARY LAYER FLOWS WITH SUCTION ACROSS A POROUS WALL

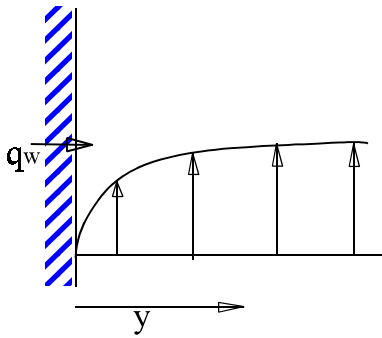


Here the U-Momentum equation reduces to :

$$\frac{\partial \tau}{\partial y} = \rho V_w \frac{\partial U}{\partial y} \quad \rightarrow \quad \frac{\partial \tau^+}{\partial y^+} = V_w^+ \frac{\partial U^+}{\partial y^+}$$

Since $V_w < 0$ (for suction) $\partial \tau^+ / \partial y^+ < 0$

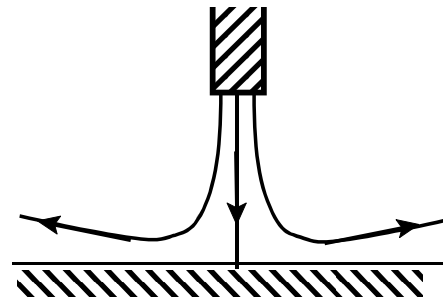
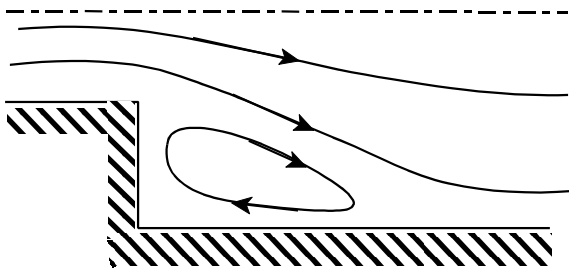
MIXED CONVECTION



Here the buoyancy force accelerates the boundary layer flow, leading to :

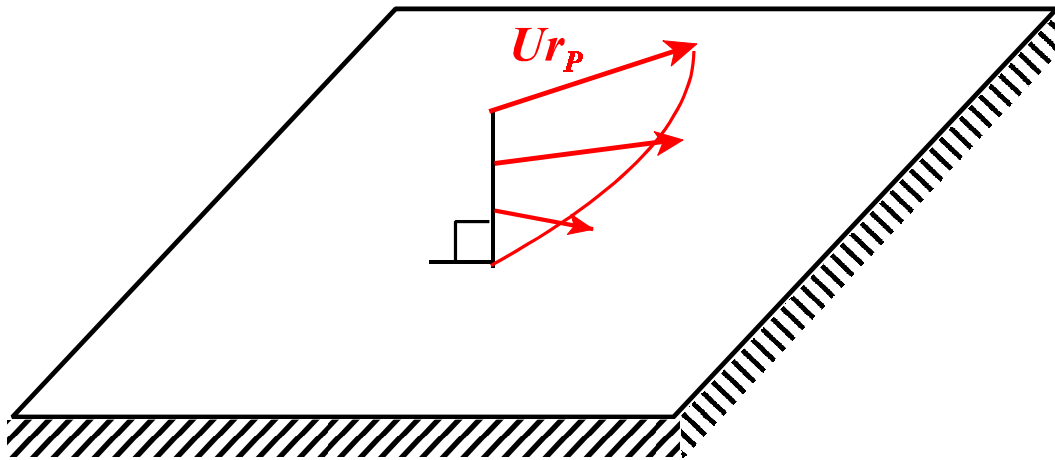
$$\frac{d\tau^+}{dy^+} \Big|_{y=0} = \frac{\nu}{\rho U_\tau^3} (\rho - \rho_{ref}) g$$

SEPARATED AND IMPINGING FLOWS



In both the above flows the near-wall velocity in the re-circulation, re-attachment and stagnation regions, would no longer obey the log-law.

THREE-DIMENSIONAL BOUNDARY LAYERS



As shown above, in a complex three-dimensional boundary layer, the resultant velocity can change its direction between the near-wall node and the solid surface.

This cannot be allowed for in the conventional wall functions.

SUMMARY OF LIMITATIONS OF CONVENTIONAL WALL FUNCTIONS.

Most assumptions involved in the conventional wall functions, break down in complex flows.

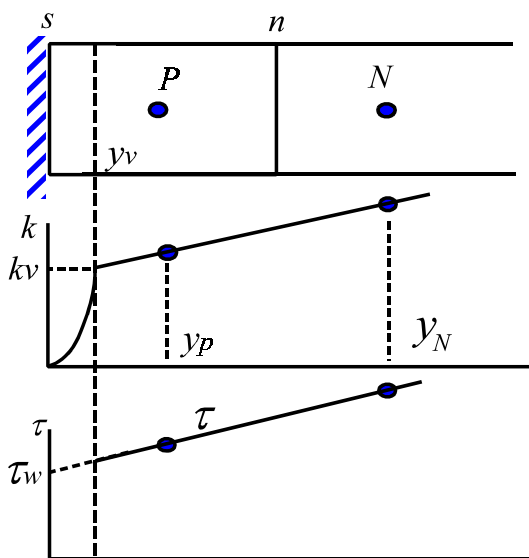
Conventional wall functions can thus result in predictions that are either inaccurate or sensitive to the size of the near-wall cells.

2. Refinements of the Conventional Wall Function

Chieng-Launder Wall Function

- **New Elements.**

In order to address some of the issues discussed above, Chieng and Launder allowed for a linear variation of the both the shear stress, τ , and of the turbulent kinetic energy, k , across the near-wall cell.



As shown in the diagram, the linear variation of k is obtained from the nodal values of k at the near-wall node, P , and the one next to it, N .

Within the viscous sub-layer, k is again assumed to have a quadratic variation.

The total shear stress, $\tau = \mu(\partial U/\partial y) - \rho uv$, is assumed to vary linearly from the wall (τ_w) to y_N (τ_N). Within the sub-layer, the contribution of the

turbulent shear stress is assumed to be negligible.

While in the "standard" approach the physical distance y_v is obtained from $y_v k_p^{1/2}/\nu = 20$, now that k varies linearly with y , **y_v is obtained from $y_v k_v^{1/2}/\nu = 20$** . This would give rise to a non-linear equation for y_v .

$$\left[k_N - \frac{k_N - k_P}{y_N - y_P} (y_N - y_v) \right]^{1/2} \frac{y_v}{\nu} = 20$$

- **Overall Approach**

The overall approach is the same as that of the "standard" wall function strategy.

Due to the refinements described above, the resulting equations, listed in the next page, are more complex.

Summary of Chieng - Launder Wall Function

$$\left[k_N - \frac{k_N - k_P}{y_N - y_P} (y_N - y_v) \right]^{1/2} \frac{y_v}{\nu} = 20$$

$$\tau_w = \kappa c_\mu^{1/4} \rho k_v^{1/2} U_p / \ln \left(E c_\mu^{1/4} y_v^* \right)$$

$$\overline{P}_k = \frac{\tau_w (U_n - U_v)}{y_n} + \frac{\tau_w (\tau_n - \tau_w)}{\kappa c_\mu^{1/4} \rho k_v^{1/2} y_n} \left(1 - \frac{y_v}{y_n} \right)$$

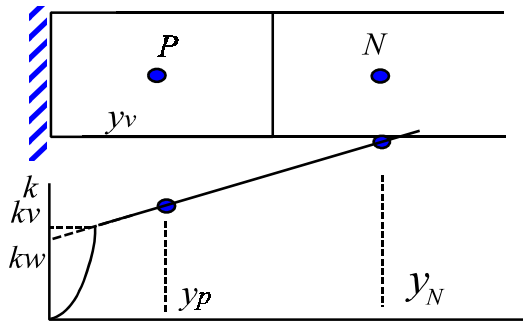
$$\overline{\epsilon} = \frac{1}{y_n} \left[\frac{2 \nu k_v}{y_v} + \int_{y_v}^{y_n} \frac{1}{c_\ell y} \left(k_n - \frac{(k_n - k_p)}{y_n - y_p} (y_n - y) \right)^{3/2} dy \right]$$

Launder and Johnson Modification

As explained earlier, one of the consequences of non-uniform shear is to alter the dimensionless thickness of the viscous sub-layer.

The Launder-Johnson modification is an attempt to take this into account.

When there is diffusion of energy towards the wall ($dk/dy > 0$) then the dimensionless thickness of the sub-layer is reduced.



By making use of k_w , the pseudo wall value of k , a parameter λ can be introduced, that represents the strength of such diffusion.

$$\lambda \equiv (k_v - k_w) / k_v$$

Then the dimensionless thickness of the sub-layer, which in equilibrium boundary layers has the value of 20, is modified according to :

$$y_v^* = 20 / (1 + c \lambda)$$

Where the coefficient, c , takes the value of 3.1.

Thus

$$\left[k_N - \frac{k_N - k_P}{y_N - y_P} (y_N - y_v) \right]^{1/2} \frac{y_v}{\nu} = \frac{20}{1 + c \lambda}$$

Comments

Tests show that the Chieng-Launder wall-function:

Improves predictions in separated and impinging flows.

Reduces sensitivity of the predictions to the size of near-wall cells.

The Launder and Johnson Modification is found to improve predictions in some cases, but can be numerically unstable.

Even with these refinements, the conventional wall functions still have to impose a semi-logarithmic variation in the near-wall velocity.

To radically expand the range of flows to which the wall-function strategy can be successfully applied, new types of wall functions are necessary.

Such types, that rely on less restricting assumptions, are discussed in the next section.

3. Advanced Wall Functions.

Origin

These are two recently developed wall-functions from the UMIST group Craft et al (2002), Craft et al (2004).

Aim

To preserve the overall framework of the wall-function strategy, but to remove some of the more limiting assumptions made, such as the log-law and the constant total shear stress.

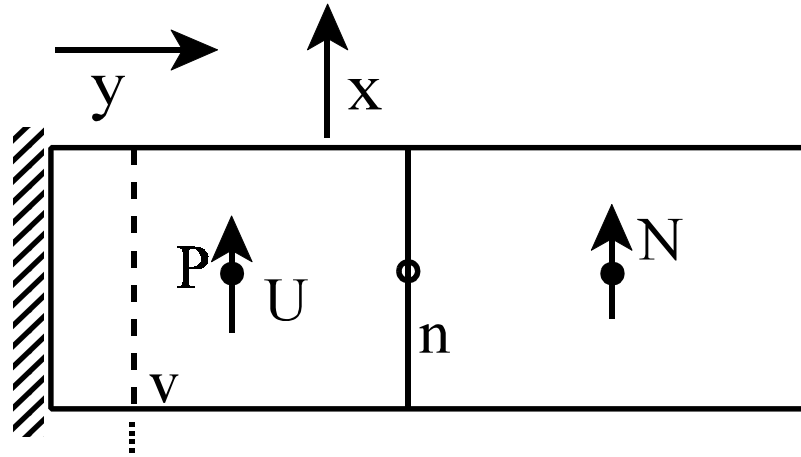
Approach

The log-law is no longer used.

The velocity and temperature variations across the near-wall cells is determined through the solution of simplified, locally one-dimensional transport equations for the wall-parallel momentum and for enthalpy.

$$\frac{d}{dy} \left[(\mu + \mu_t) \frac{dU}{dy} \right] = - \frac{d}{dx} (\rho U U) - \frac{dP}{dx} \quad (I)$$

$$\frac{d}{dy} \left[\left(\frac{\mu}{Pr} + \frac{\mu_t}{\sigma_T} \right) \frac{dT}{dy} \right] = - \frac{d}{dx} (\rho U T) \quad (II)$$



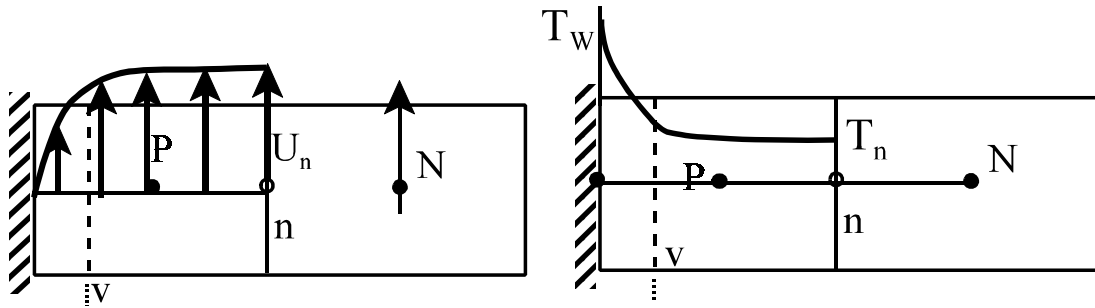
Where x and y the wall-parallel and wall-normal directions respectively.

Boundary conditions are:

$$\text{At } y = 0, \quad U=0 \quad T=T_w$$

$$\text{At } y = y_n \quad U_n = (U_P + U_N)/2 \quad T_n = (T_P + T_N)/2$$

Solution of these two equations will result in the velocity and temperature distribution across the near-wall cells.



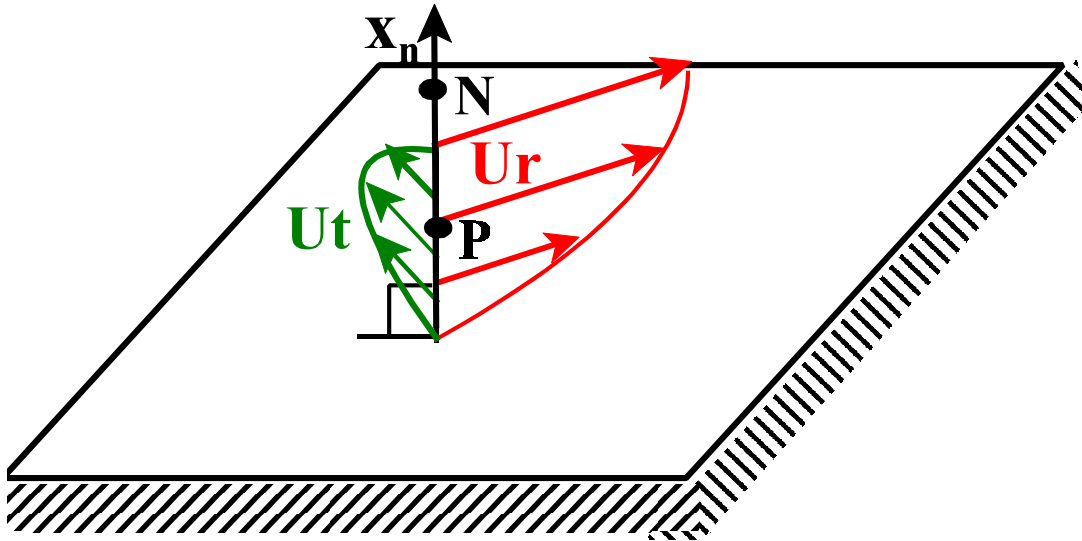
From these distributions the wall shear stress, τ_w , and also either the wall temperature, T_w , or the wall heat flux, q_w , (depending on the thermal boundary conditions) can be obtained.

The wall shear stress and either, T_w or q_w can then be used to modify the discretized momentum and enthalpy equations over the near-wall cells, as in the conventional wall-functions.

The velocity distribution can also be used to produce the average generation rate of turbulence, P_k , across the near-wall cells

The average P_k is then used to modify the discretized k equation over the near-wall cell, as in the conventional wall functions.

In three-dimensional flows, momentum transport equations in two directions can be independently solved.



$$\frac{d}{dx_n} \left[(\mu + \mu_t) \frac{dU_r}{dx_n} \right] = - \frac{d}{dx_r} (\rho U_r U_r) - \frac{dP}{dx_r} \quad (Ia)$$

$$\frac{d}{dx_n} \left[(\mu + \mu_t) \frac{dU_t}{dx_n} \right] = - \frac{d}{dx_t} (\rho U_t U_t) - \frac{dP}{dx_t} \quad (Ib)$$

$$\text{At } x_n = 0 \quad U_n = 0 \quad U_t = 0$$

$$\text{At } x_n = x_n^n \quad U_n = 0.5 * (U_n^P + U_n^N) \quad U_t = 0$$

- **Alternative Strategies**

The solution of equations (I) and (II) requires the introduction of further assumptions.

The two different strategies that have been developed at UMIST that:

- Share the same overall approach outlined so far.
- Differ in the assumptions used and the methods employed to solve equations (I) and (II).
- Both come under the acronym of UMIST, here denoting *Unified Modelling through Integrated Sub-layer Transport*.

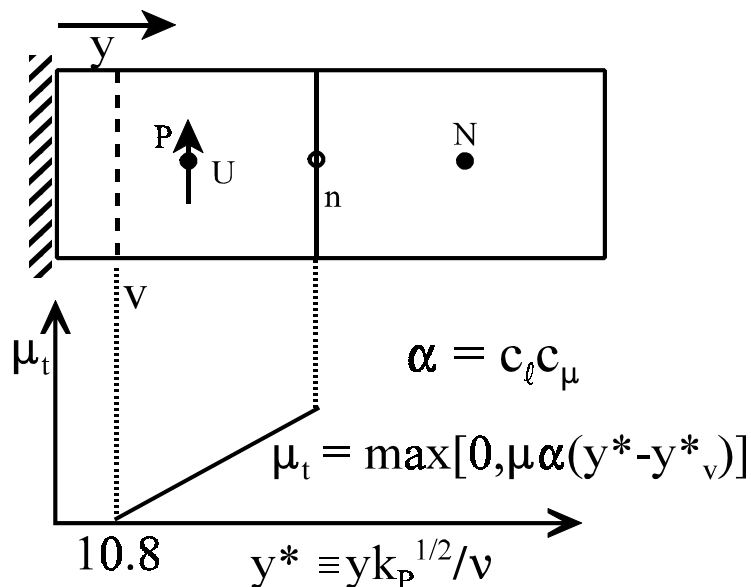
The two alternatives are now separately presented.

3.1 The Analytical Wall Function, UMIST-A

- **Mean Flow Analysis**

As the name implies, **equations (I) and (II) are solved analytically** across the near-wall cell.

This is accomplished through the use of a **prescribed variation for the turbulent viscosity, μ_t .**



A consequence of the above variation in μ_t , is that two forms of equations (I) and (II) are solved.

For $y^* < y_v^*$

$$\mu \frac{d}{dy} \left[\frac{dU}{dy} \right] = \left[\frac{d}{dx} (\rho U U) + \frac{dP}{dx} \right]_P$$

$$\frac{\mu}{Pr} \frac{d}{dy} \left[\frac{dT}{dy} \right] = \left[\frac{d}{dx} (\rho U T) \right]_P$$

For $y_v^* > y^* < y_n^*$

$$\mu \frac{d}{dy} \left[\left(1 + \alpha (y^* - y_v^*) \right) \frac{dU}{dy} \right] = \left[\frac{d}{dx} (\rho U U) + \frac{dP}{dx} \right]_P$$

$$\frac{\mu}{Pr} \frac{d}{dy} \left[\left(1 + \frac{\alpha Pr}{\sigma_T} (y^* - y_v^*) \right) \frac{dT}{dy} \right] = \left[\frac{d}{dx} (\rho U T) \right]_P$$

The right hand sides of the equations are treated as constants and are calculated from the nodal values.

At the interface between the two regions, y_v^* , it is required that the variables (U and T) and their first derivatives (dU/dy and dT/dy) are continuous.

The empirical constant y_v^* is determined as **10.8**

The analytical integration of the above equations results in the following U distribution across the near-wall cells.

$$\text{For } y^* < y_v^* \quad U = \frac{A_U y^*}{\mu} + \frac{C_U y^{*2}}{2\mu}$$

For $y_v^* > y^* < y_n^*$

$$U = \frac{C_U}{\mu\alpha} y^* - \frac{C_U \lambda}{\mu\alpha^2} \ln(Y^*) + \frac{A_U}{\mu\alpha} \ln(Y^*)$$

$$+ \frac{A_U y_v^*}{\mu} + \frac{C_U y_v^*}{\mu} \left(\frac{y_v^*}{2} - \frac{1}{\alpha} \right)$$

Where

$$A_U = \frac{\left[\mu U_n - C_U \left(\frac{1}{\alpha} (y_n^* - y_v^*) + \frac{y_v^{*2}}{2} - \frac{1}{\alpha^2} \lambda \ln[Y_n^*] \right) \right]}{y_v^* + \frac{1}{\alpha} \ln[Y_n^*]}$$

$$C_U = \frac{v^2}{k_p} \left[\frac{d}{dx} (\rho U U) + \frac{dP}{dx} \right]_P$$

$$(1 - \alpha y_v^*) \equiv \lambda \quad \text{and} \quad 1 + \alpha (y_n^* - y_v^*) \equiv Y^*$$

Similarly the temperature distribution is.

$$\text{For } y^* < y^*_v \quad T = \frac{A_T y^*}{\mu/Pr} + \frac{C_T y^{*2}}{2\mu/Pr} + T_W$$

For $y^*_v > y^* < y^*_n$

$$\begin{aligned} T = T_W + \frac{Pr}{\mu\alpha_T} C_T y^* - \frac{Pr}{\mu\alpha_T^2} C_T \lambda_T \ln(Y^*_T) + \frac{Pr}{\mu\alpha_T} A_T \ln(Y^*_T) \\ + \frac{Pr}{\mu} A_T y^*_v + \frac{Pr}{\mu} C_T y^*_v \left(\frac{y^*_v}{2} - \frac{1}{\alpha_T} \right) \end{aligned}$$

Where

$$A_T = \frac{\left[\frac{\mu}{Pr} (T_n - T_W) - C_T \left(\frac{1}{\alpha_T} (y^*_n - y^*_v) + \frac{y^{*2}_v}{2} - \frac{1}{\alpha_T^2} \lambda_T \ln[Y^*_{Tn}] \right) \right]}{y^*_v + \frac{1}{\alpha_T} \ln[Y^*_{Tn}]}$$

$$C_T = \frac{v^2}{k_p} \left[\frac{d}{dx} (\rho UT) \right]_P$$

$$(1 - \alpha_T y^*_v) \equiv \lambda_T \quad \text{and} \quad 1 + \alpha_T (y^* - y^*_v) \equiv Y^*_T$$

- **Wall Shear Stress and Wall Heat Flux**

Differentiation of the above expressions at $y=0$, will then result in expressions for the wall shear stress and the wall heat flux.

$$\tau_w = -\mu dU/dy_{y=0} \quad \text{and} \quad q_w = - (c_p \mu / Pr) dT/dy_{y=0}$$

- **Average Generation Rate, P_k**

$$P_k = \mu_t [dU/dy]^2 \quad \text{and} \quad \mu_t = \alpha \mu (y^* - y_v^*)$$

$$\text{Thus :} \quad P_k = \alpha \mu (y^* - y_v^*) [dU/dy]^2$$

Integration leads to:

$$\bar{P}_k = \frac{\alpha \mu}{y_n} \int_{y=y_v}^{y=y_n} (y^* - y_v^*) \left(\frac{dU}{dy} \right)^2 dy$$

Where dU/dy is obtained by differentiating the expression for U , over the region $y > y_v$.

- **Average Dissipation Rate**

As in the conventional wall-functions

For $y < y_d$: $\epsilon = 2 \nu k_p / y_d^2$

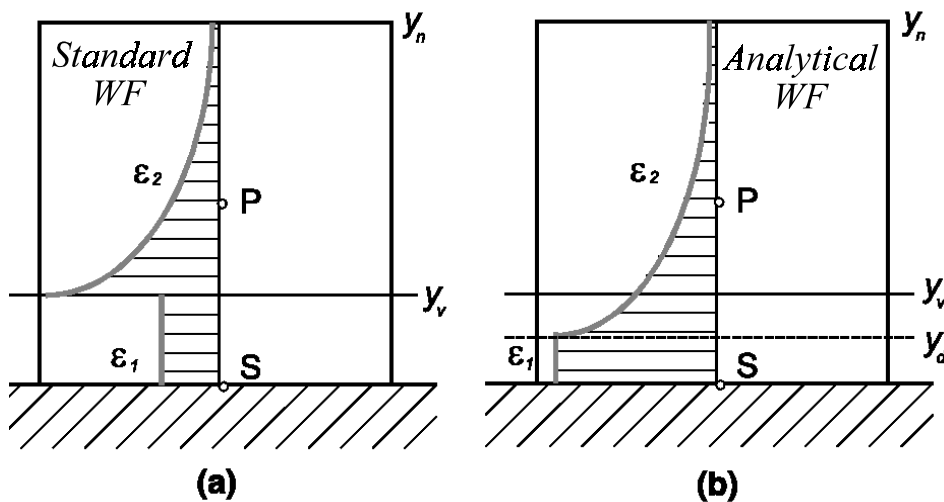
For $y > y_d$: $\epsilon = k_p^{3/2} / c_\ell y$

Unlike the conventional wall functions, case (a):

$$y_d^* \neq y_v^* (=20)$$

For continuity of ϵ : $2 \nu k_p / y_d^2 = k_p^{3/2} / c_\ell y_d$

→ $y_d^* = 5.1$



Thus
$$\bar{\epsilon} = \frac{k_p^{3/2}}{y_n} \left[\frac{2}{y_d^*} + \frac{1}{c_\ell} \ln \left(\frac{y_n}{y_d} \right) \right]$$

- **Further Extensions**

The assumptions involved in the Analytical Wall Function are less restrictive than those in the conventional wall functions.

It is consequently possible to introduce further refinements to the Analytical Wall Function to extend the range of flows that it can be applied.

These refinements include.

- Introduction of Laminarization Effects
- Temperature Variation of Viscosity
- Inclusion of Buoyancy Effects
- High Prandlt Number Modification
- Extension to flows over rough surfaces.

Some of the above refinements make the resulting equations more complex, but because they are still algebraic equations, the associated computational overheads are negligible.

Inclusion of Laminarization Effects

Objective is similar to that in Johnson-Launder.

The availability of the analytical velocity variation, makes it possible to employ a more convenient local parameter, λ

$$\lambda = \tau_w / \tau_v$$

Then the average dissipation rate is multiplied by the function F_ϵ .

$$\overline{\epsilon}_{NEW} = F_\epsilon \overline{\epsilon}_{ORIGINAL}$$

$$\lambda \geq 1 \quad F_\epsilon = 1 + 1.5 \{ 1 - \exp[-6.9(\lambda - 0.98)] \} \\ \{ 1 - \exp[-193(\max(\alpha, 0))^2] \}$$

$$\lambda < 1 \quad F_\epsilon = 1 - (1 - F_{\epsilon 0}) [1 - \exp(-(1 - \lambda)/\lambda)] \\ \{ 1 - \exp[-11.1(\max(\gamma, 0))^2] \}$$

$$\alpha = (\lambda / 1.02) - 1 \quad \gamma = 0.98 / \lambda \quad F_{\epsilon 0} = 0.75$$

When $\lambda > 1$, $F_\epsilon > 1 \rightarrow$ thicker viscous sub-layer.

When $\lambda < 1$, trend is reversed.

Temperature Variation of Viscosity

In strongly heated flows, changes in temperature cause variations in fluid properties (viscosity and thermal conductivity) across the near-wall cells.

These changes can have a strong effect on hydrodynamic and thermal boundary layers.

Temperature, and hence fluid properties, change most strongly across the viscous sub-layer.

Thus, only changes in fluid properties across the zero-viscosity-region are taken into account.

$$\text{For } y < y_v \quad \mu = \frac{\mu_w}{1 + b_\mu y^* (y^* - 2y_v^*)}$$

$$\text{Where } b_\mu = \frac{1}{y_v^{*2}} \left(1 - \frac{\mu_w}{\mu_v} \right)$$

With μ_w and μ_v the viscosities at the analytical solution temperatures, at the wall and the edge of the zero-turbulent-viscosity sub-layer.

Inclusion of Buoyancy Effects

The effects of the buoyancy force can be included at two different levels.

- ▲ In the analytical solution of the wall-parallel moment equation

$$\frac{d}{dy} \left[(\mu + \mu_t) \frac{dU}{dy} \right] = \left[\frac{d}{dx} (\rho U U) + \frac{dP}{dx} \right]_P + \rho_{ref} g_x \beta (T - T_{ref})$$

Where T is based on the analytical solution of the enthalpy equation.

- ▲ The integrated form of the buoyancy force, across the near-wall control volume, can be calculated and included in the discretized form of the wall-parallel momentum equation over the near-wall control volume.

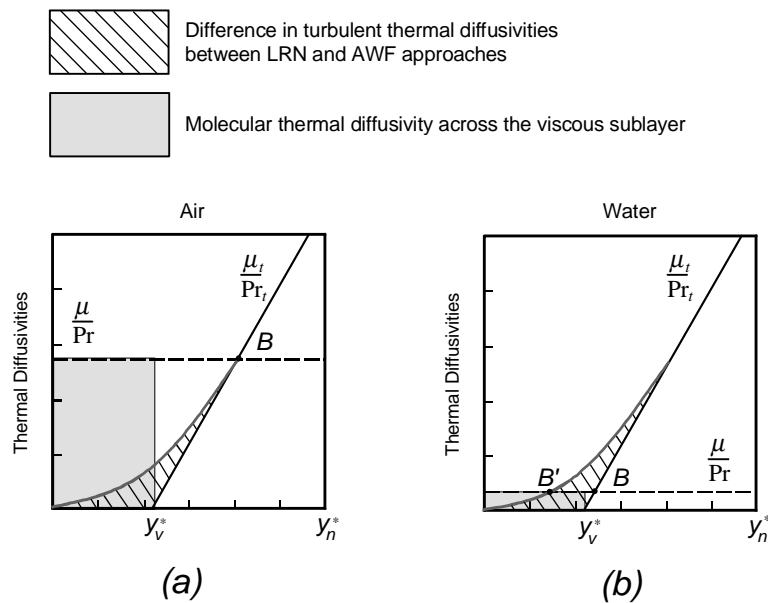
$$\overline{F_{bx}} = \frac{1}{y_n} \int_{y_n}^{y_n} \rho_{ref} g_x \beta (T - T_{ref}) dy$$

Both the above extensions become possible, because of the availability of the analytical temperature variation over the near-wall cells.

High Prandtl Number Modification.

At high Prandtl numbers the sub-layer, across which turbulent transport of thermal energy is negligible, becomes thinner than the viscous sub-layer.

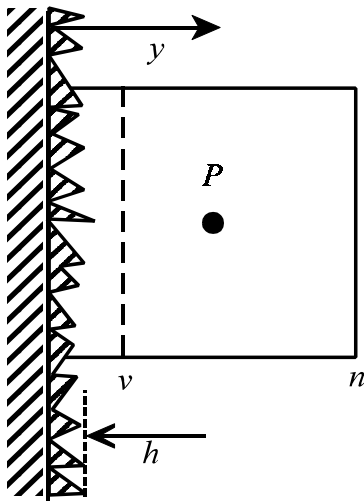
Thus, the assumption that the turbulent heat flux becomes negligible when $y < y_v$, no longer applies.



This is corrected, through the introduction of an effective molecular Prandtl number in equation (II).

$$\text{Pr}_{eff} = \frac{\text{Pr}}{1 + 0.017 \cdot \text{Pr} \cdot [1 + 2.9 |F_\varepsilon - 1|]^{1.5}}$$

Extension to flows over rough surfaces



- Average height of roughness elements : h

N



- Local Dimensionless height of roughness elements at near-wall node P: $h^* \equiv h k_P^{0.5} / \nu$

- Surface roughness affects the modelling of near-wall turbulence modifying the dimensionless thickness of the viscosity-dominated sub-layer, y_v^* .

For a smooth surface : $y_{vs}^* = 10.7$

For a rough surface :

$$y_v^* = y_{vs}^* [1 - (h^*/70)^m]$$

Where m is empirically determined.

• Applications of the Analytical Wall Function

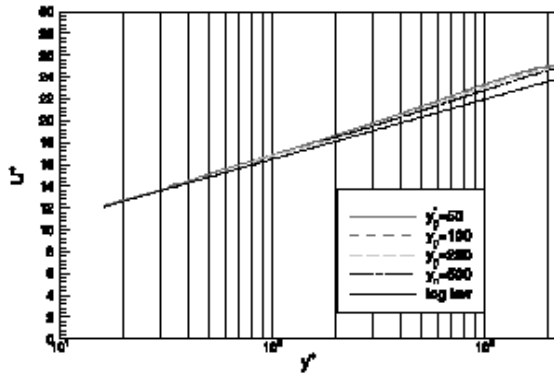


Fig. 8. Semi-logarithmic velocity profiles for $Re = 100,000$ for isothermal fully developed pipe flow.

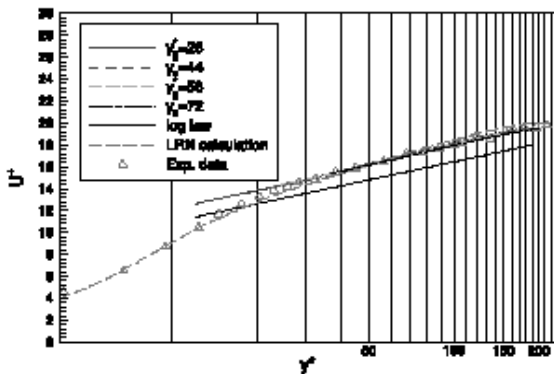
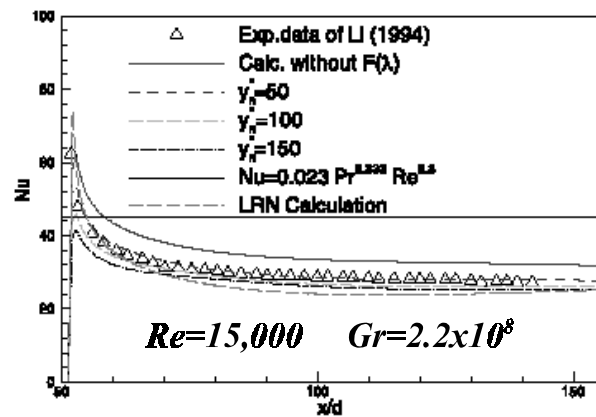
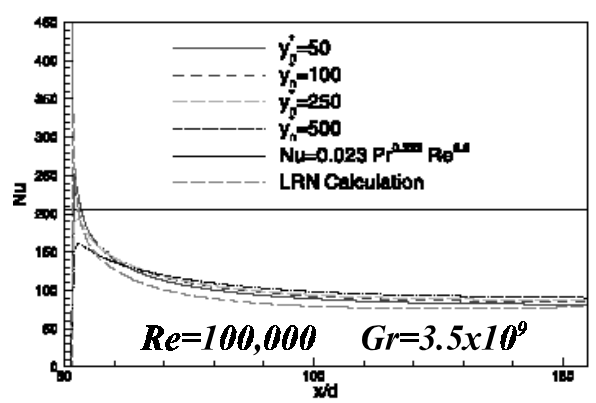


Fig. 9. Semi-logarithmic velocity profiles for $Re = 6753$ for isothermal fully developed pipe flow.



Fully Developed Pipe Flows

Developing Mixed-Convection, Upward Pipe Flows

Annular Buoyancy-Opposed Flows

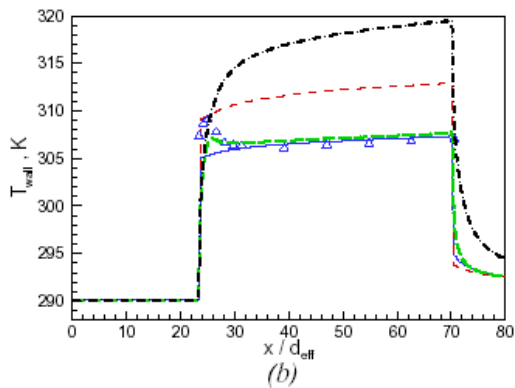
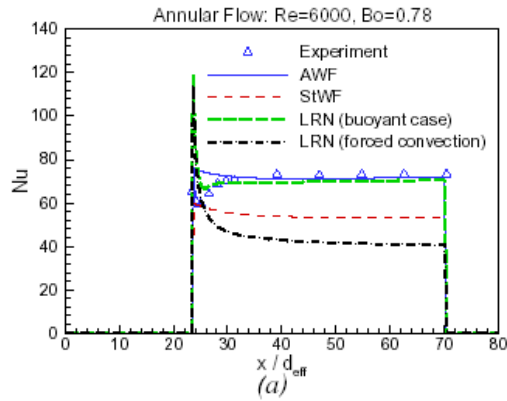
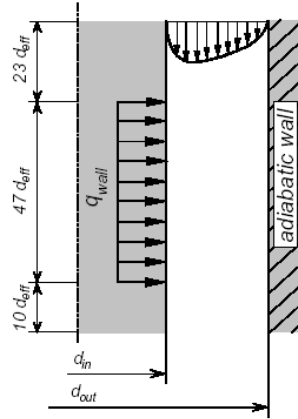


Figure 6. Predicted (a) Nusselt number and (b) wall temperature for buoyancy-opposed water flow in annulus at $Bo=0.78$.

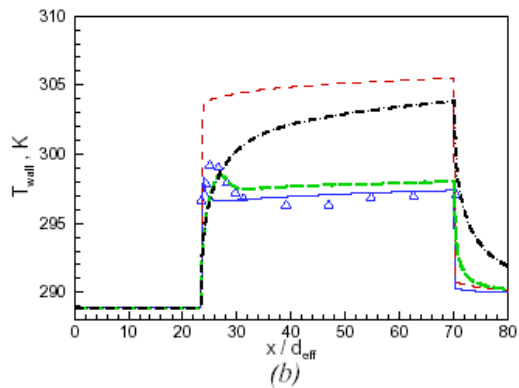
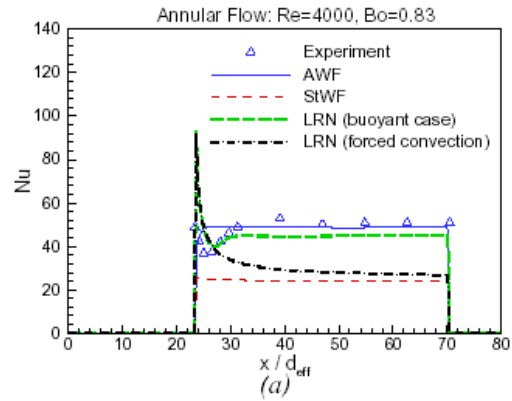
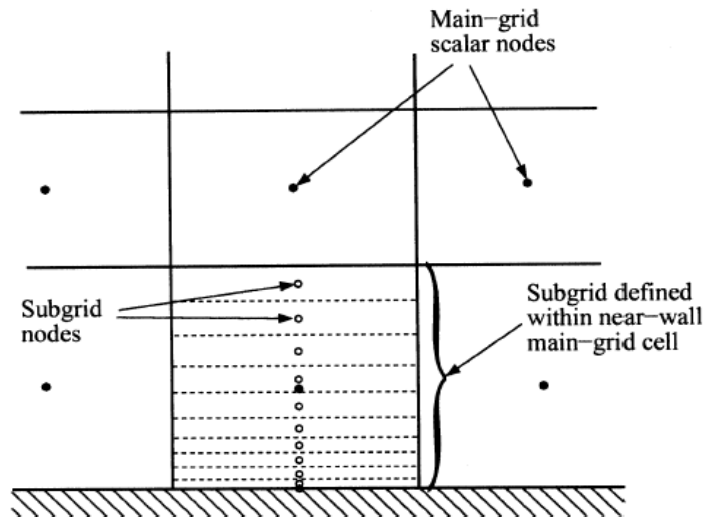


Figure 7. Predicted (a) Nusselt number and (b) wall temperature for buoyancy-opposed water flow in annulus at $Bo=0.83$ and $Re=4000$.

3.2 The Numerical Wall Function, UMIST-N

The simplified transport equations for the wall-parallel momentum and enthalpy are numerically solved across the near-wall cells.

- Each near-wall cell is divided into a number of sub-volumes.



$$\frac{d}{dy} \left[(\mu + \mu_t) \frac{dU}{dy} \right] - \frac{d}{dy} (\rho VU) = \left[\frac{d}{dx} (\rho UU) + \frac{dP}{dx} \right]_P$$

$$\frac{d}{dy} \left[\left(\frac{\mu}{Pr} + \frac{\mu_t}{\sigma_t} \right) \frac{dT}{dy} \right] - \frac{d}{dy} (\rho VT) = \left[\frac{d}{dx} (\rho UT) \right]_P$$

- Left hand side terms are discretized using sub-grid nodal values.

- Right hand side terms are discretized using main grid nodal values and are constant across each cell.

- The wall normal velocity at the sub-grid nodes is obtained from local sub-cell continuity.

- The turbulent viscosity at the sub-grid nodes is determined by numerically solving simplified equations of a low-Reynolds-number model.

- If the Launder-Sharma is used, for example:

$$\frac{\partial}{\partial y}(\rho V k) + \left[\frac{\partial}{\partial x}(\rho U k) \right]_P = \frac{\partial}{\partial y} \left[(\mu + \mu_t) \frac{\partial k}{\partial y} \right] + P_k - \rho \epsilon - 2\rho \nu \left(\frac{\partial \sqrt{k}}{\partial y} \right)^2$$

$$\frac{\partial}{\partial y}(\rho V \epsilon) + \left[\frac{\partial}{\partial x}(\rho U \epsilon) \right]_P = \frac{\partial}{\partial y} \left[(\mu + \mu_t) \frac{\partial \epsilon}{\partial y} \right]$$

$$+ c_{\epsilon 1} \frac{\epsilon}{k} P_k - \rho c_{\epsilon 2} f_2 \frac{\epsilon^2}{k} + 2\rho \nu \nu_t \left[\frac{\partial^2 U}{\partial y^2} \right]^2 + YC$$

Terms with subscript P evaluated using main grid nodal values.

$$\mu_t = \rho c_\mu f_\mu k^2 / \epsilon \quad P_k = \mu_t (dU/dy)^2$$

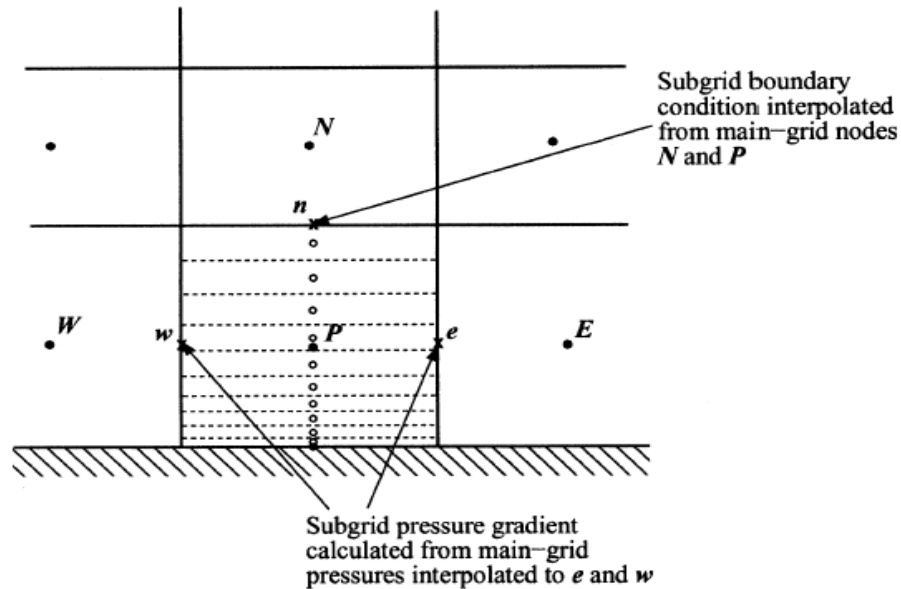
$$f_2 = 1 - 0.3 \exp(-R_t^2) \quad f_\mu = \exp[-3.4 / (1 + 0.02 R_t^2)]$$

$$R_t = k^2 / (\nu \epsilon)$$

YC denotes the Yap length scale correction term.

- **Implementation**

- The sub-grid nodal values of the flow variables are stored for all near-wall cells.



- The discretization of the wall-parallel convection $\rho U(d\Phi/dx)$ is thus based on sub-grid nodal values.
- The discretization of the simplified transport equations within each near-wall cell, results in a tri-diagonal system.

$$\rho V \frac{\partial \Phi}{\partial y} - \frac{\partial}{\partial y} \left(\Gamma \frac{\partial \Phi}{\partial y} \right) = S'_{\Phi} \equiv S_{\Phi} - \rho U \frac{\partial \Phi}{\partial x}$$

$$\rightarrow A_P \Phi_P = A_N \Phi_N + N \Phi_N + S'_{\Phi}$$

- Within each near-wall cell, the discretized sub-grid equations are solved using a tri-diagonal matrix solver.

- Only one sweep of the sub-grid TDMA is performed within each iteration.
- The k and ϵ equations are under-relaxed.

- Following each sub-grid iteration, the sub-grid nodal values are used to produce the following:

- **Wall Shear Stress** τ_w , used to modify the discretized wall-parallel momentum equation at the near-wall cells
- Either the **wall temperature**, T_w or the **wall heat flux**, q_w , that modify the enthalpy equation at the near-wall cells.
- The **cell-averaged** P_k and ϵ that modify the k transport equation at the near-wall cells.
- The **cell-averaged**

$$c_{\epsilon 1} \frac{\epsilon}{k} P_k - \rho c_{\epsilon 2} f_2 \frac{\epsilon^2}{k} + 2\rho \nu v_t \left[\frac{\partial^2 U}{\partial y^2} \right]^2 + YC$$

that modify the discretized ϵ equation at the near-wall cells.

This wall-function strategy can be used with other low-Re models, such as non-linear $k-\epsilon$ models.

- **Applications of the Numerical Wall Function**

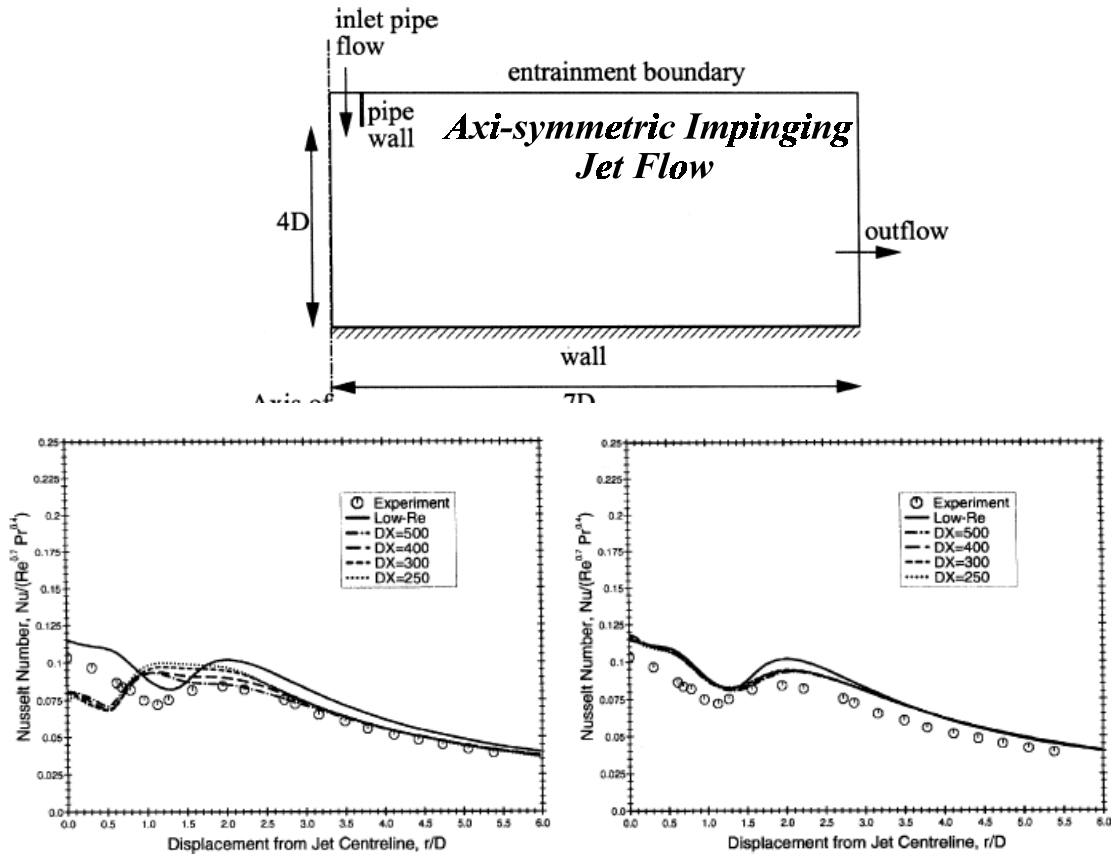


Figure 5. Nusselt number predictions for the impinging jet ($H/D = 4, Re = 70,000$) using the nonlinear $k-\epsilon$ model; broken lines are wall-function results with different near-wall cell sizes; (left) Chieng and Launder wall function; (right) UMIST- N wall function.

	Wall functions		
	Chieng and Launder	UMIST- N	Low-Re, Craft et al.
Number of nodes	70×45	$70 \times 45 (+ 40)$	70×90
CPU time per iteration (s)	0.158	0.260	0.324
No. of iterations	1,426	1,380	9,116
Total CPU time (s)	226	359	2,955
Relative CPU time	1	1.59	13.08

Free Rotating Disc Flow

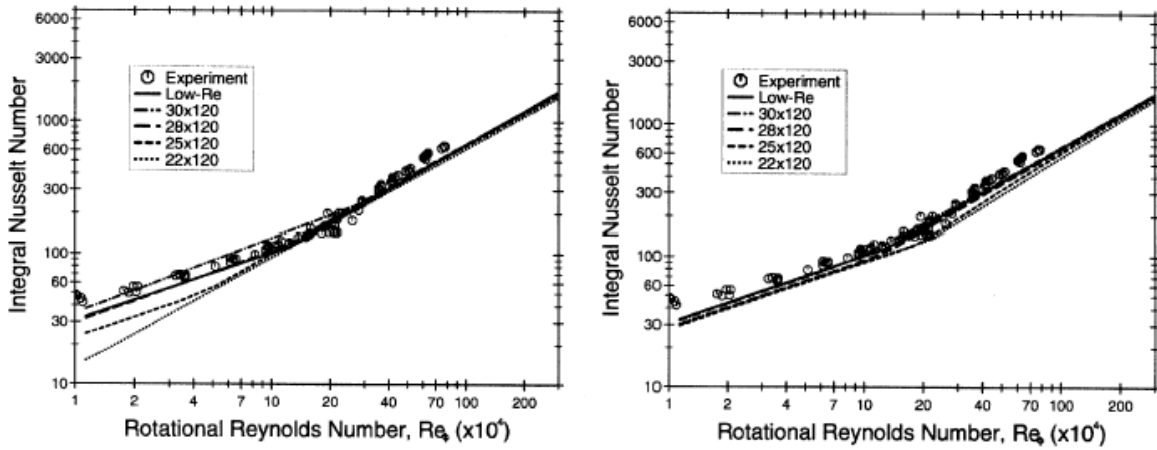
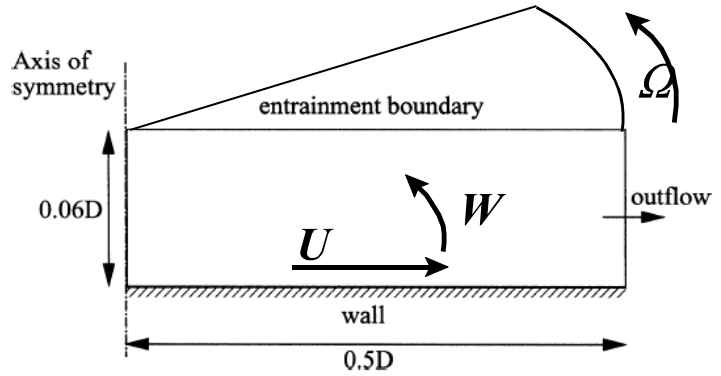


Figure 8. Predicted integral Nusselt number in the free-disc flow using the linear $k - \epsilon$ model with: (left) Chieng and Launder wall function; (right) UMIST- N wall function. Solid line, low-Re model; broken lines, wall function results for different grid arrangements; \circ , experimental values from Cobb and Saunders [24].

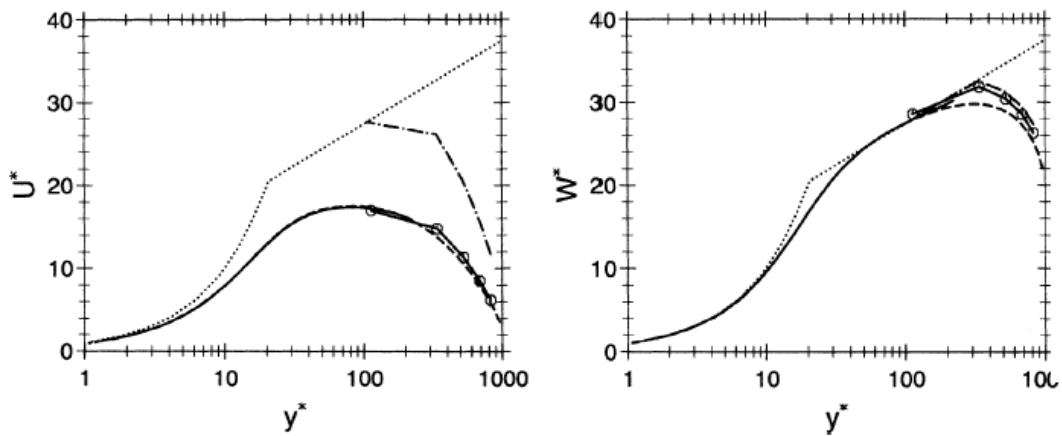


Figure 9. Velocity profiles for the free-disc flow at $Re_\phi = 1.0 \times 10^6$ using wall-law axes; (left) radial U -velocity and (right) tangential W -velocity; \circ , UMIST- N wall function (circles indicate the position of primary grid nodes and the solid line without symbols represents the solution across the subgrid); ---, low-Re model; - - -, Chieng and Launder wall function; · · ·, "universal" log-law.

4. Concluding Remarks

- Some Weaknesses of the conventional wall functions have been identified.
- Extensions of the conventional wall functions have been presented.
- Two recently developed wall-function strategies have been presented, which instead of relying on the log-law, solve simplified momentum and enthalpy equations across the near-wall cells.
 - The Analytical Wall Function, UMIST-A, is as computationally efficient as the conventional approach and in many complex flows results in predictions of the same quality as a low-Reynolds-number approach.
 - The Numerical Wall Function, UMIST-N, while increasing computational overheads, relative to the conventional approach, by 60% to 100%, results in predictions similar to those of low-Re models at only a fraction of the cost.

REFERENCES

Chieng C C and Launder B E (1980). *On the calculation of turbulent heat transport downstream from an abrupt pipe expansion.* Numerical Heat Transfer, **vol 3**, pp 189-207.

Johnson R W and Launder B E (1982). *Discussion of 'On the calculation of turbulent heat transport downstream from an abrupt pipe expansion.'* Numerical Heat Transfer, **vol 5**, pp 493-496.

T. J. Craft, A Gerasimov, H. Iacovides and B.E. Launder
Progress in the generalisation of wall-function treatments.
International Journal of Heat and Fluid Flow, **23**,
148-16,2002

T. J. Craft., S. E. Gant, H. Iacovides and B. E. Launder
A New Wall-Function strategy for Complex Turbulent Flows.
Numerical Heat Transfer. Part B: Fundamentals, **45**,
No 4, pp 301-318, 2004

T.J. Craft, A. V. Gerasimov, H. Iacovides, J. W. Kidger and B. E. Launder

The Negatively Buoyant Turbulent Wall Jet: Performance of alternative options in RANS Modelling.. Accepted, International Journal of Heat and Fluid Flow, 2004.

K. Suga, T.J. Craft, H. Iacovides

Extending an analytical wall-function for turbulent flows over rough walls.

ETMM6, ERCOFTAC International Symposium on Engineering Turbulence Modelling and Measurements, Sardinia, Italy, May 23-25, 2005.

H. Iacovides

June 2004